Journal of Alloys and Compounds 504 (2010) 457–461

Contents lists available at ScienceDirect

Journal of Alloys and Compounds

journal homepage: www.elsevier.com/locate/jallcom

Synthesis and characterization of tin dioxide/multiwall carbon nanotube composites

Chuanqi Feng[a,*], Li Li[a], Zaiping Guo[b], Hua Li[a]

[a] College of Chemistry and Chemical Engineering, Hubei University, Wuhan 430062, PR China
[b] School of Mechanical, Materials & Mechatronic Engineering, University of Wollongong, Wollongong, NSW 2522, Australia

ARTICLE INFO

Article history:
Received 16 November 2009
Received in revised form 22 May 2010
Accepted 29 May 2010
Available online 11 June 2010

Keywords:
Electrode materials
Inorganic composite materials
Chemical synthesis
Electrochemical reactions
X-ray diffraction

ABSTRACT

Nanocomposites composed of tin dioxide/multiwall carbon nanotubes (MWCNTs) were synthesized by a chemical precipitation method. The content of SnO_2 in the nanocomposites was adjusted by changing the mass ratio of $SnCl_4{\cdot}4H_2O$ to MWCNTs. The crystalline structure and morphology of the as-prepared samples were characterized by X-ray diffraction (XRD) and transmission electron microscopy (TEM). The electrochemical properties of the composites were investigated with a battery testing system. The results show that the electrochemical performance of a composite is strongly dependent on the content of SnO_2 in the composites. A nanocomposite containing 50 wt.% of SnO_2 gave the best performance, exhibiting relatively higher reversible capacity (523 mAh/g) and excellent cycling ability. The possible reasons why the composite has such an outstanding electrochemical performance are discussed also.

1. Introduction

Lithium-ion batteries are considered to be the most promising power sources for various portable electronic device applications. The search for materials with improved electrochemical properties is one of the important research topics in the area of lithium batteries. Tin dioxide in glassy, amorphous and crystalline forms has extensively studied since tin dioxide electrode materials were first reported by Fuji Film scientists in 1995 [1]. These materials, relying on the formation of Li_xSn ($0 \le x \le 4.4$) alloys, exhibited higher specific capacity (781 mAh/g) [2,3] than the conventional graphite anodes in commercial use. The disadvantage of tin dioxide as an anode in Li-ion cells is its poor cycling stability which results from mechanical failure and loss of electrical activity of the electrode due to the drastic volume change between Sn and $Li_{4.4}Sn$ (about 358%) [4–7].

In order to alleviate the volume changes, various methods have been investigated, such as modification of SnO_2 nanostructures [8,9], synthesis of tin dioxide in three-dimensional (3D) porous amorphous form [10], and adding/coating with buffer materials (such as carbon or other conductive materials) inside or outside the particles [11,12]. Recently, the use of composites has become a very important issue in finding a solution to the problem of the large capacity fade observed for these anode materials after cycling. Xiao et al. reported that SnO_2/Mg_2SnO_4 nanocubes synthesized by the hydrothermal method had a higher capacity and better cyclability compared to pure SnO_2 or Mg_2SnO_4 [13]. Yang et al. used solid-state reaction to synthesize SnO_2/NiO nanomaterials whose maximum specific capacitance was 357.45 F/g, according to their cyclic voltammetry (CV) results [14]. Chou et al. used carbon from the decomposition of sucrose as a support matrix to prepare carbon-coated SnO_2 nanocomposites, and the cycling stability was improved in comparison with bare metal electrodes [15].

Carbon nanotubes can act as a barrier to suppress the aggregation and pulverization of active particles and thus increase their structural stability during cycling [16,17]. Furthermore, the carbon nanotube has a high electronic conductivity and it can improve the conductance of the active materials [18]. In addition, ductile carbonaceous materials could absorb the mechanical stress caused by the volume change, therefore, synthesis of the SnO_2/multiwalled carbon nanotubes (MWCNTs) nanocomposite is an effective way to improve the electrochemical performance including the reversible capacity and cycling performances compared with pure SnO_2.

In this work, SnO_2/MWCNT nanocomposites were synthesized by a chemical precipitation method, and the electrochemical properties of the nanocomposites as anode materials for lithium-ion batteries are reported.

2. Experimental

2.1. Synthesis of the samples

The MWCNTs raw material was first refluxed in 2 mol/L HNO_3 for 6 h at 110 °C, and then the solution was neutralized and filtrated. The filtrated sample was soaked

* Corresponding author. Tel.: +86 27 88666486; fax: +86 27 88663043.
E-mail address: pfcq@263.net (C. Feng).

0925-8388/$ – see front matter © 2010 Published by Elsevier B.V.
doi:10.1016/j.jallcom.2010.05.144

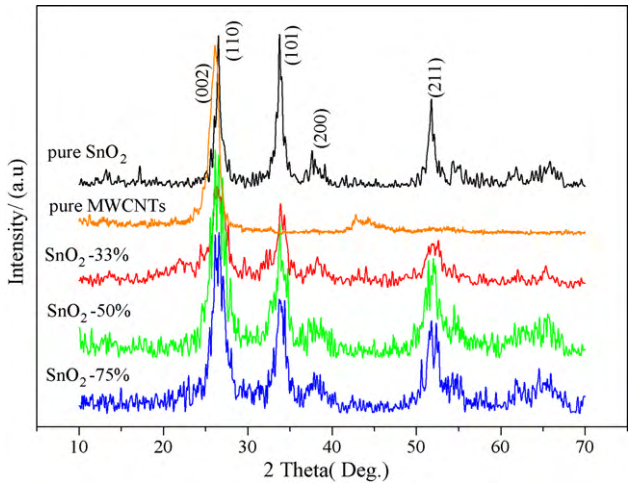

Fig. 1. XRD patterns of pure SnO_2, MWCNTs and SnO_2-containing nanocomposites.

in H_2O_2 for 24 h. Finally, the solution was again filtered and subsequently washed with distilled water and alcohol several times until the pH value reached at about 7. This was followed by drying at 100 °C for more than 10 h under vacuum.

The SnO_2/MWCNTs composites were obtained by chemical precipitation method. Typically, calculated amounts of $SnCl_4{\cdot}4H_2O$ and MWCNTs were dissolved in distilled water in turn. The suspension was sonicated for 30 min, and $NH_3{\cdot}H_2O$ solution was added by drop until the pH value reached at 3 under continuous and vigorous stirring for 30 min with the ultrasonic vibrations. The resultant precipitate was centrifuged and subsequently rinsed with large amounts of distilled water, then alcohol. This was followed by an overnight drying under vacuum at 80 °C. Finally, the compound was heat-treated at 400 °C for 2 h in a tube furnace under air to achieve the thermal decomposition of the precipitate and allow metal oxide formation to be accomplished. The prepared samples are denoted as SnO_2-*X*% nanocomposites, where *X* is the SnO_2 content in the nanocomposite. The final products had three different tin oxide content levels and are denoted as SnO_2-33%, SnO_2-50% and SnO_2-75%. Pure SnO_2 was also synthesized by the same method in the absence of MWCNTs.

2.2. Characterization of samples

Powder X-ray diffraction (XRD,Rigaku D/max-ra) using Cu Ka radiation (λ = 1.540 6 Å) with a graphite monochromator was employed to identify the crystalline phase of the synthesized materials. The morphology of the resulting compound was observed using a transmission electron microscope (TEM, Philip, Technai).

2.3. Electrochemical tests

Charge–discharge tests were performed using CR2016 coin-type cell in an automatic battery tester system (Neware, China). The working electrode was formulated from a mixture of 60 wt.% of the nanocomposites, 30 wt.% of acetylene black and 10 wt.% of polytetrafluoroethylene (PTFE) binder. Lithium foil was used as the counter electrode, and the electrolyte was 1 M $LiPF_6$ in a mixture of ethylene carbonate (EC) and dimethyl carbonate (DMC) (1:1, v/v). All test cells were assembled in an argon-filled glove box containing less than 1 ppm each of oxygen and moisture. The cells were discharged and charged at a constant current of 40 mA/g over a voltage range of 0.01–3.00 V vs. Li/Li^+ at room temperature. The typical masses of electrode materials used in the experimental were from 5 to 8 mg.

3. Results and discussion

3.1. Structure and morphology characterization

XRD was used to characterize the microcrystalline structure of these nanocomposites (33 wt.%SnO_2, 50 wt.%SnO_2 and 75 wt.%SnO_2), and the XRD patterns are presented in Fig. 1. As a comparison, the XRD patterns of the bare MWCNTs and nanocrystalline SnO_2 are also presented in Fig. 1. Some peaks originate from the MWCNTs and SnO_2 diffractions can be clearly observed. We can also observe that the XRD patterns of the nanocomposites are clearly different from the peaks of MWCNTs and the bare SnO_2, but it can be seen that XRD patterns of all nanocomposites are overlap of the patterns of cassiterite SnO_2 (JCPDS No. 72-1174) and graphite (JCPDS No.75-1621). The three typical diffraction peaks at $2\theta = 26.6°$, 34°, 54° of the bare SnO_2, and the prominent (0 0 2) diffraction peak at $2\theta = 26°$ of the graphite continue to be present in the patterns of the nanocomposites, although the widths of the main peaks of the nanocomposites are broadened, so the composites are thus proved to be formed from MWCNTs and nanocrystalline SnO_2 [19]. Using the Scherrer equation, the mean particle sizes of the nanocomposites (33 wt.%SnO_2, 50 wt.%SnO_2, and 75 wt.%SnO_2) are calculated to be about 9.9, 10, and 12 nm, respectively, which is almost in agreement with the results from TEM in Fig. 2.

The TEM morphologies of the pure SnO_2 and SnO_2-containing nanocomposites are presented in Fig. 2. It can be seen that the pure SnO_2 is composed of tiny nanoparticles with a grain size of ~15 nm. In the case of the SnO_2-containing nanocomposites, the carbon nanotubes are entangled together, and SnO_2 nanoparticles with sizes of only a few nanometers (~10 nm) are dispersed in the carbon nanotubes matrix. With increasing SnO_2 content, the SnO_2 nanoparticles on the surface of the MWCNTs show a greater tendency towards aggregation, although the nanocrystallites in the SnO_2/MWCNT sample with the greatest tin dioxide content, as shown in Fig. 2d, can still be clearly seen. The chemical precipitation method can thus lead to the formation of small homogeneous clusters of SnO_2 particles on MWCNT support.

3.2. Electrochemical properties

Fig. 3 shows the charge/discharge profiles of the nanocomposite samples, along with the pure SnO_2 and MWCNTs, cycled between 0.01 and 3.00 V at a current density of 40 mA/g. In Fig. 3a, the pure MWCNTs exhibited two sloping discharge plateaus at ~1.7 and ~0.8 V in the first discharge curve, the first of which corresponds to reduction of impurity resulting from the decomposition of the solvent in the electrolyte solution and the formation of a solid electrolyte interphase (SEI) layer, which leads to some consumption of Li^+ ions. In the second cycle, the discharge plateau is located at about 0.5 V. The discharge plateau at ~1.7 V corresponds to reduction of impurities resulting from decomposition of the solvent in the electrolyte solution, As the reduction reaction is irreversible, the discharge plateau at higher potential (1.7 V) observed in the first cycle has disappeared, as is verified in the discharge/charge curves of Fig. 3.

As shown in Fig. 3b for the pure SnO_2, there is a plateau around 0.8 V in the first cycle, which is ascribed to the reduction of SnO_2 to metallic Sn and Li_2O, and the formation of a solid electrolyte interphase (SEI) layer. A sloping voltage profile in the range of 0.01–1.00 V is also found during the second discharge pattern, which is attributed to the lithium insertion into Sn formed during the first lithium insertion and corresponds to the phase transitions between LiSn, Li_2Sn, Li_7Sn_3, Li_5Sn_2, and $Li_{22}Sn_5$ [20]. A plateau at around 0.4 V was observed during the second charge process, which is an indication of a de-alloying reaction of Li–Sn alloys formed during the discharge. The electrochemical reaction mechanism of Li with SnO_2 in lithium-ion batteries can be described in the following Eqs. (1) and (2) [4]:

$$SnO_2 + 4Li^+ + 4e^- \rightarrow Sn + 2Li_2O \quad (1)$$

$$Sn + xLi^+ + xe^- \leftrightarrow Li_xSn (0 \le x \le 4.4) \quad (2)$$

During the 10th cycle, we observed that the discharge/charge plateaus have become shorter than in the second cycle. This phenomenon can be explained by the following factors: during the cycling process, the nano-Sn particles are inclined towards aggregation and pulverization, which severely degrades their structural stability. Therefore, lithium insertion into and extraction from the

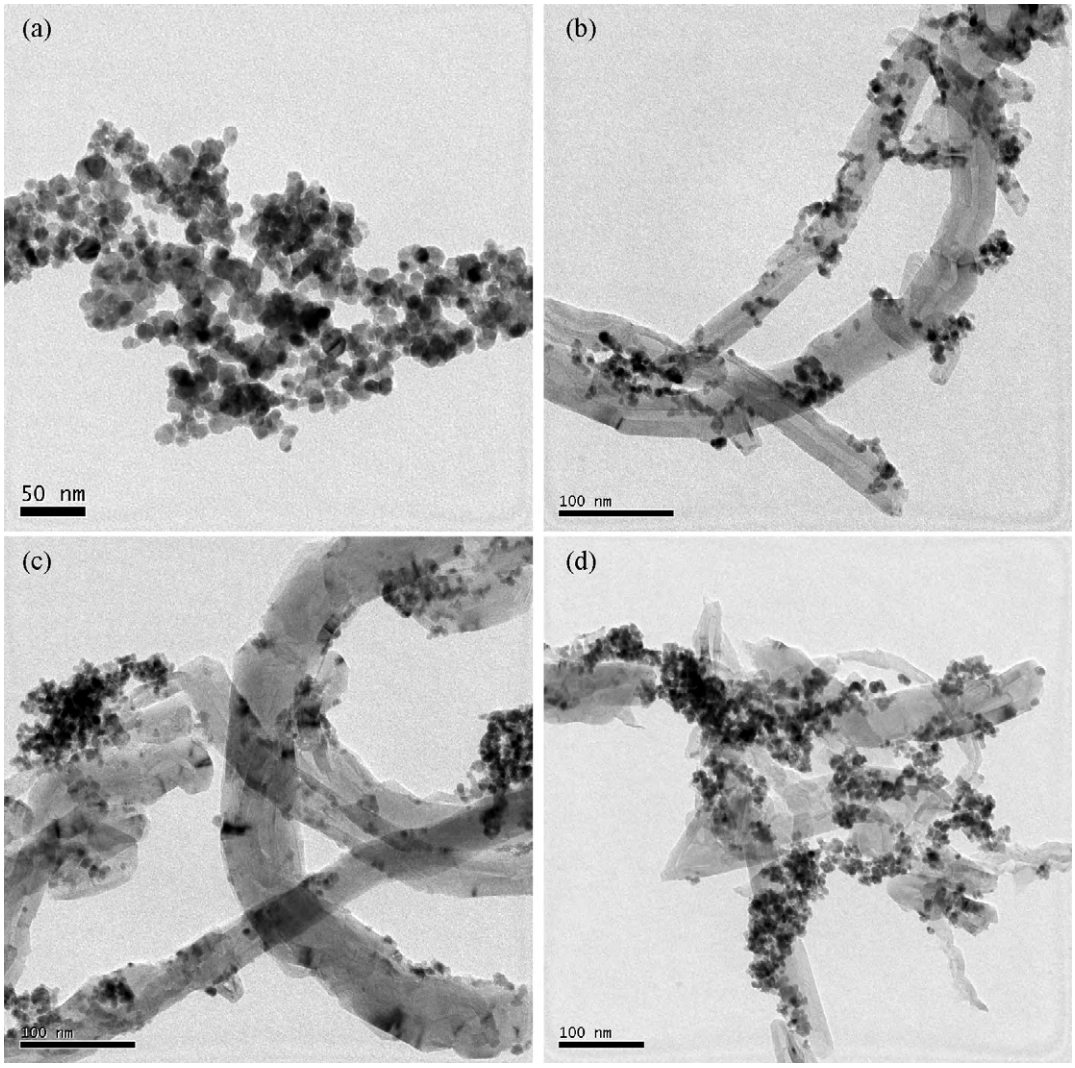

Fig. 2. TEM images of samples (a) pure SnO_2, (b) SnO_2-33% nanocomposite, (c) SnO_2-50% nanocomposite and (d) SnO_2-75% nanocomposite.

host matrix becomes extremely difficult. Hence, it is not advisable to use nanocrystalline SnO_2 alone as an electrode active material in Li-ion cells. Compared with Fig. 3a and b, the discharge/charge patterns of the SnO_2/MWCNTs (Fig. 3c, d and e) are similar to those of the pure SnO_2 and MWCNTs. Taking the example of Fig. 3d, during the second discharge cycle, the sloping voltage profile at 0.01–1.00 V may be ascribed to the formation of the complex $Li_{22}Sn_5$ phase, with part of the Li^+ being inserted into the layer of MWCNTs [21]. According to the XRD patterns, the composite is composed of pure SnO_2 and MWCNTs, and the MWCNTs and SnO_2 both have the ability to intercalate Li^+ as an electrode material in the nanocomposite. Thus, the discharge/charge patterns of SnO_2/MWCNTs should overlap the patterns of the MWCNTs and the pure SnO_2.

From Fig. 3c–e, we observe that there is a trend towards a falling discharge voltage plateau and a simultaneous increase in the charge voltage with the increasing SnO_2 content. This demonstrates that the electrochemical performance is strongly dependent on the content of SnO_2 in the nanocomposites, and the MWCNT matrix should play a key role in the good cycling performance of the nanocomposites. With increasing SnO_2 content, there is a high probability that the the nano-Sn particles will aggregate, but the relatively few MWCNTs in the matrix may be incapable of buttering the large volume changes, so that the highest SnO_2 sample featured poor cycling performance. So, it is very important to choose a moderate proportion of SnO_2 in the SnO_2/MWCNTs in order to obtain excellent electrochemical properties such as high capacity and good cycling performances.

Fig. 4 shows the cycling behaviors of MWCNTs, pure SnO_2, and the SnO_2/MWCNT composite (c, d and e) electrodes in constant current charge/discharge mode. The initial discharge capacity of pure SnO_2 and SnO_2/MWCNT composites (c, d and e) come from four contributions: chemical Li^+ insertion, non-chemical Li^+ insertion (where lithium ions intercalate into defect sites in the nanomaterial), the formation of an SEI layer, and the insertion of Li^+ into acetylene black. However, in our experiment, the initial discharge capacity is calculated according to mass of SnO_2 (mg) or mass of composite (mg), which could result in a calculated initial discharge capacity that is higher than actual initial discharge capacity of the SnO_2 or the initial discharge capacity of the composites. Nevertheless, it is difficult to explain why our initial discharge capacities are so high just from the theoretical capacities of SnO_2 and MWCNTs.

The bare MWCNTs electrode is very stable on cycling, but with limited capacity: the initial discharge specific capacity is 1075 mAh/g, and after 20 cycles, the discharge capacity still retains a value of 335 mAh/g, which is about 74% of the second discharge capacity (453 mAh/g). The bare nanocrystalline SnO_2 anode has a high first discharge capacity (2013 mAh/g), however, its capac-

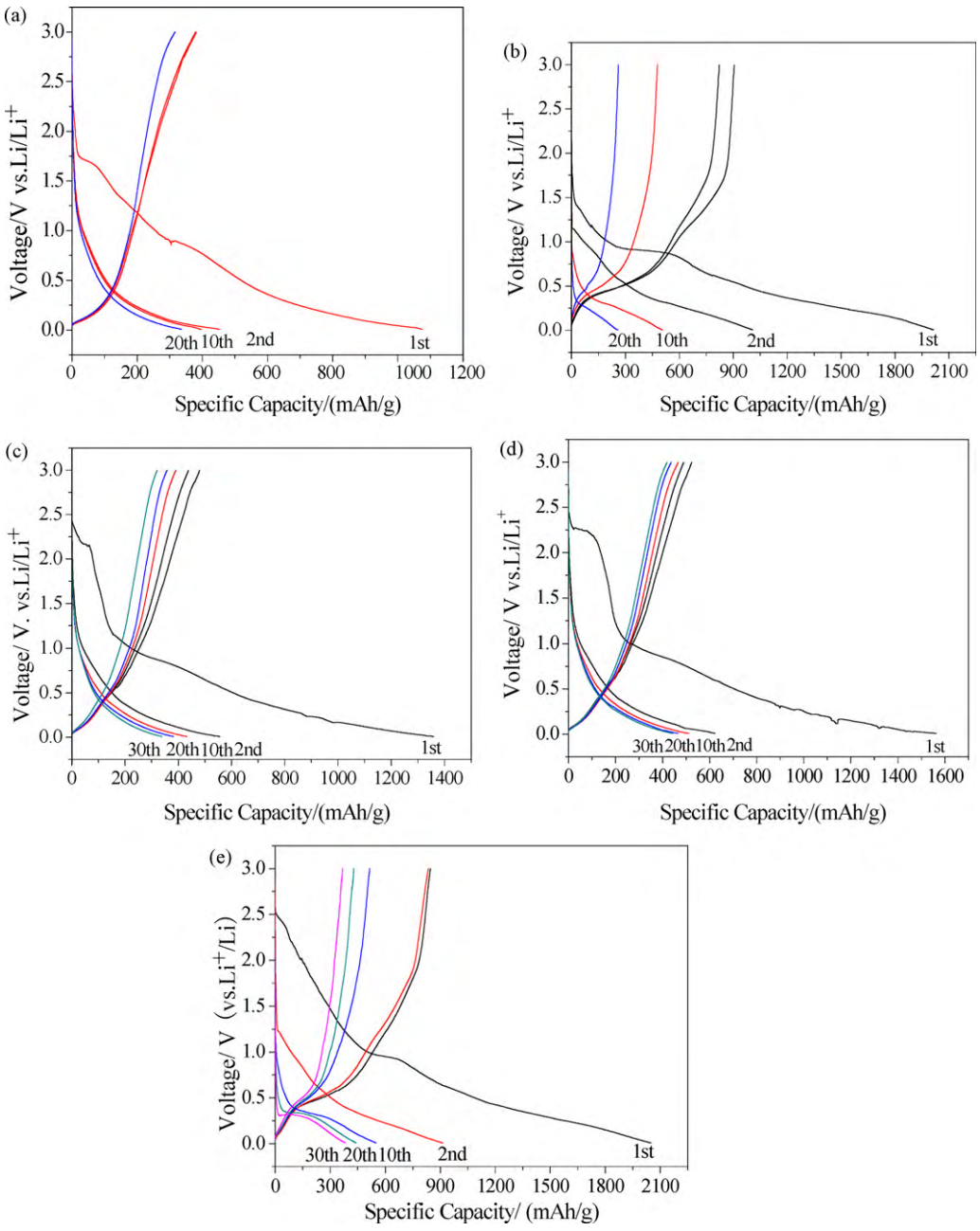

Fig. 3. The discharge/charge curve of the samples cycled between 0.01 and 3.00 V at 40 mA/g (a) pure MWCNTs, (b) pure SnO_2, (c) SnO_2-33%, (d) SnO_2-50% and (e) SnO_2-75%.

ity fades rapidly during cycling, and the discharge capacity is 1003 mAh/g during the second cycle, so the capacity fades especially severely in the first cycle. The discharge capacity is only 257 mAh/g after 20 cycles. Although bare SnO_2 has a high initial discharge capacity, it has very inferior cycling stability, and therefore, nanocrystalline SnO_2 alone is unsuitable for electrodes in Li-ion cells. Compared with the pure MWCNTs and SnO_2, the nanocomposites showed relatively better electrochemical properties. Nanocrystalline SnO_2-33% exhibits good cycling stability, but low capacity. The initial discharge specific capacity is 1359 mAh/g, but after 30 cycles, the discharge capacity is only 337 mAh/g. Meanwhile, nanocrystalline SnO_2-75% has extraordinarily high capacity, but extreme deterioration in the cycling performance: the initial discharge specific capacity is 2049 mAh/g, but after 30 cycles, the discharge capacity is only 382 mAh/g. However, compared to bare MWCNTs, bare nano-SnO_2 electrodes and the other two nanocomposites, nanocrystalline SnO_2-50% composite electrode demonstrated outstanding performance (high capacity and satisfactory cycling stability). The initial discharge specific capacity is 1562 mAh/g, and the SnO_2-50% electrode shows good cycling stability, with only 1% capacity loss per cycle from the second to the 30th cycle. The discharge capacity for SnO_2-50% after 30 cycles is 442 mAh/g, which is 71% of the second discharge capacity, so in order to improve the capabilities of MWCNTs and the cycling stability of SnO_2, it is a valid approach to synthesize a nanocomposite of pure SnO_2 and MWCNTs, while the ratio of SnO_2 to MWCNTs is also a key factor affecting the electrochemical performance of the nanocomposite.

During the discharge process, the formation of Li–Sn alloy induces a large volume increase, which could create micro-cracks and therefore destroy the integrity of the electrode, causing high irreversible capacity and poor cycling stability in bare SnO_2 elec-

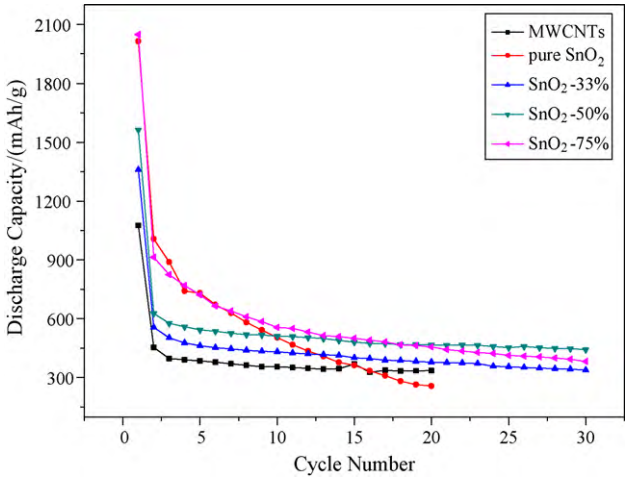

Fig. 4. The cycle patterns of the samples cycled in the voltage range of 0.01–3.00 V at 40 mA/g.

trode. In comparison, the integrity of the SnO_2-50% nanocomposite in the electrode could be preserved under repeated lithium insertion and extraction. The reasons can be attributed to the following aspects: firstly, the tubular organization of MWCNTs limits the mobility of particles during cycling [22]; secondly, the ductile MWCNT matrix surrounding the nano-SnO_2 clusters improves the stability of tin oxide particles against agglomeration [23] and provides good buffering against the local volume changes in the Li–Sn alloying and de-alloying reactions [24], so as a result, the volume changes on the macro-domain are negligibly small for SnO_2-50% electrodes; and thirdly, the good electrical conductivity of MWCNTs is also of benefit for keeping the SnO_2 nanoparticles electrically connected during the entire charging and discharging process. In addition, MWCNTs are also an active material, which can offer extra capacity to improve the overall capacity. Therefore, nano-alloy composites with MWCNTs should be a valid method to practically overcome an important obstacle to Li-alloy anode materials. Considering the high reversible capacity and good cycling stability of the as-prepared SnO_2/MWCNT nanocomposite electrodes, SnO_2/MWCNTs could be a promising alternative anode material for lithium-ion batteries.

4. Conclusions

Nanocomposites (tin dioxide–multiwall carbon nanotubes) have been synthesized from MWCNTs and $SnCl_4{\cdot}4H_2O$ by a chemical precipitation method. The SnO_2 nanoparticle content of the composite was optimized by changing the mass ratio of $SnCl_4{\cdot}4H_2O$ to MWCNTs in order to produce the most promising SnO_2/MWCNT nanocomposite with the best electrochemical properties. The results made it clear that the SnO_2-50% nanocomposite exhibited the highest reversible storage capacity, as well as the most stable cycling performance. Since this synthetic method is simple and convenient, it can meet the growing demand for large-scale production of tin dioxide nanocomposite anode materials.

Acknowledgments

Financial support provided by the Australian Research Council (ARC) through an ARC Discovery project (DP0878611) and Project of Education Department of Hubei (D20101006) is gratefully acknowledged. Moreover, the authors would like to thank Dr. Tania Silver at the University of Wollongong for critical reading of the manuscript.

References

[1] Y. Idota, T. Kubota, A. Matsufuji, Y. Maekawa, T. Miyasaka, Science 276 (1997) 1395–1397.
[2] J. Xie, V.K. Varadan, Proc. SPIE 5389 (2004) 210–220.
[3] N. Li, C.R. Martin, B. Scrosati, J. Power Sources 97–98 (2001) 240–243.
[4] I.A. Courtney, J.R. Dahn, J. Electrochem. Soc. 144 (1997) 2045–2052.
[5] T. Brousse, R. Retoux, U. Herterich, D.M. Schleich, J. Electrochem. Soc. 145 (1998) 1–4.
[6] J.M. Tarascon, M. Armand, Nature 414 (2001) 359–367.
[7] J.O. Besenhard, J. Yang, M. Winter, J. Power Sources 68 (1997) 87–90.
[8] S.L. Chou, J.Z. Wang, H.K. Liu, S.X. Dou, Electrochem. Commun. 11 (2009) 242.
[9] H. Bastami, E. Taheri-Nassaj, J. Alloys Compd. 495 (2010) 121–125.
[10] Y. Yu, L. Gu, A. Dhanabalan, C.H. Chen, C.L. Wang, Electrochim. Acta 54 (2009) 7227–7230.
[11] L.M. Fang, X.T. Zu, Z.J. Li, S. Zhu, C.M. Liu, W.L. Zhou, L.M. Wang, J. Alloys Compd. 454 (2008) 261–267.
[12] M.S. Park, Y.M. Kang, J.H. Kim, G.X. Wang, S.X. Dou, H.K. Liu, Carbon 46 (2008) 35–40.
[13] T. Xiao, Y.W. Tang, Z.Y. Jia, S.L. Feng, Electrochim. Acta 54 (2009) 2396–2401.
[14] H. Yang, Q.F. Tao, X.C. Zhang, A.D. Tang, J. Ouyang, J. Alloys Compd. 459 (2008) 98–102.
[15] S.L. Chou, J.Z. Wang, C. Zhong, M.M. Rahman, H.K. Liu, S.X. Dou, Electrochim. Acta 54 (2009) 7519–7524.
[16] J. Fan, T. Wang, C. Yu, B. Tu, Z. Jiang, D. Zhao, Adv. Mater. 16 (2004) 1432–1436.
[17] L.J. Fu, H. Liu, H.P. Zhang, C. Li, T. Zhang, Y.P. Wu, R. Holze, H.Q. Wu, Electrochem. Commun. 8 (2006) 1–4.
[18] Y. Wang, F. Su, J.Y. Lee, X.S. Zhao, Chem. Mater. 18 (2006) 1347–1353.
[19] H.P. Liu, D.H. Long, X.J. Liu, W.M. Qiao, L. Zhan, L.C. Ling, Electrochim. Acta 54 (2009) 5782–5788.
[20] M. Winter, J.O. Besenhard, Electrochim. Acta 45 (1999) 31–50.
[21] Z.P. Guo, Z.W. Zhao, H.K. Liu, S.X. Dou, Carbon 43 (2005) 1392–1399.
[22] Y. Wang, J.Y. Lee, H.C. Zeng, Chem. Mater. 17 (2005) 3899–3903.
[23] Y. Wang, J.Y. Lee, J. Phys. Chem. B 108 (2004) 17832–17837.
[24] K.T. Lee, Y.S. Jung, S.M. Oh, J. Am. Chem. Soc. 125 (2003) 5652–5653.